The role of cellular instability on the critical tube diameter problem for unstable gaseous detonations

Han Xu [1,2], Xiaocheng Mi [2], Charles B. Kiyanda [3], Hoi Dick Ng [3†], John H.S. Lee [2] and Chunde Yao [1]

[1] Tianjin University
State Key Laboratory of Engines (SKLE), Tianjin University, Tianjin, P. R. China, 300072

[2] McGill University
Department of Mechanical Engineering, Montreal, QC H3A 2K6, Canada

[3] Concordia University
Department of Mechanical, Industrial and Aerospace Engineering, Montreal, QC H3G 1M8, Canada

[†]Corresponding Author

Department of Mechanical, Industrial and Aerospace Engineering
Concordia University
Montreal, QC H3G 1M8, Canada
e-mail: hoing@encs.concordia.ca
Tel.: 1 (514) 848-2424 ext. 3177
Fax: 1 (514) 848-3175

Revised Manuscript submitted to the Proceedings of the Combustion Institute
37th Symposium (International) on Combustion
Colloquium: Detonations, Explosions and Supersonic Combustion

Preferred type of presentation: oral

Total length of paper (method 1): 6125
Main text: 3398
Equations: 46
References: 542
Figure 1 with captions: 85
Figure 2 with captions: 175
Figure 3 with captions: 156
Figure 4 with captions: 249
Figure 5 with captions: 174
Figure 6 with captions: 174
Figure 7 with captions: 398
Figure 8 with captions: 151
Figure 9 with captions: 170
Figure 10 with captions: 142
Figure 11 with captions: 265

We agree to pay charges for reproduction of color figures.

May 2018

Abstract

The transmission of detonation waves, propagating in a homogeneous, gaseous, reactive medium, from a tube into an unconfined space is well known to succeed or fail based on the tube diameter. Below a certain diameter, the detonation fails to transition into the unconfined space, while for a large enough geometry, the transition succeeds. This critical diameter is well correlated to the incoming detonation cell size. For common undiluted hydrocarbon mixtures with strong degree of transverse instability, the ratio of critical tube diameter to cell size has been measured at $D_c = 13\lambda$. In this paper, stoichiometric acetylene-oxygen mixture at different initial pressures is detonated in a circular tube that transitions into an effectively unconfined space. The transition is observed with simultaneous Schlieren photography and soot foil records to look at the role of transverse cellular instability. Three regimes of transition are observed: supercritical, where the cellular pattern is continuously connected from the donor tube to the larger space; subcritical, where the wave fails and the cellular pattern disappears; and a critical regime, where the wave initially fails, asymptoting to a weakly decoupled shock-reaction front regime, and exhibits a subsequent re-initiation in a critical zone of pre-shocked gas through the onset of an explosion bubble. A substantial amount of transverse instability remains even after the expansion wave reaches the central axis, sustaining the diffracted wave at a critical thermodynamic state for the re-initiation. The location of this critical zone is identified at about 22λ and a small obstacle is used to promote the generation of transverse waves and a re-initiation kernel. The re-initiation is effected by placing an obstacle in the critical region. The role of the resulting instability is also illustrated through a simple numerical simulation using an obstacle in the sub-critical regime to perturb the flow and promote the re-initiation.

Keyword: detonation; diffraction; critical tube diameter; instability; transverse waves

1. Introduction

When a detonation wave diffracts from a confined tube with a diameter D into an open area, it fails if D is below a critical tube diameter, D_c. Besides its direct relevance to the design of detonation-based propulsion systems [1], the critical tube diameter phenomenon has been a classical problem to understand the dynamics of detonations, and their failure and initiation mechanisms.

It has been established that D_c can be used as an alternative length scale that provides an assessment of a combustible mixture's detonation sensitivity, and correlates well with other detonation dynamic parameters, e.g., the detonation cell size or the critical energy for direct initiation [2-6]. Except for "stable", highly argon diluted combustible mixtures [7], the empirical law $D_c \sim 13\lambda$ applies to most common gaseous hydrocarbon mixtures with an "unstable" cellular detonation front, i.e., embedded with small scale instabilities and irregular transverse waves [3, 4]. For stable mixtures with a very regular front structure, the critical conditions vary significantly with $D_c \sim 20$ to 30λ [8-10]. The difference in scaling between regular and irregular mixtures suggests different detonation failure mechanisms.

A number of studies have aimed at revealing the fundamental detonation failure mechanism in the critical tube diameter problem. In particular, Lee [11] conjectured two modes of detonation diffraction failure. For stable detonations, failure is predominantly caused by excessive front curvature, distributed over the global detonation surface by corner expansion waves. Above a critical curvature, the ZND-like detonation cannot maintain the global coupling between the leading front and the reaction zone. A recent numerical study [12] showed that for a stable detonation with regular cellular pattern, the two-dimensional critical channel width and critical diameter differ by a factor close to 2, equal to the geometrical scaling based on front curvature theory. This mechanism is consistent with He & Clavin's curvature model [13] for detonation initiation failure, however insufficient to accurately predict the critical initiation energy experimentally measured for many common hydrocarbon, irregular mixtures. For unstable detonations, Lee therefore conjectured that failure is predominantly linked to the

suppression of instabilities or disappearance of transverse waves by corner expansion as a result of the diffraction process. Successful transmission thus invariably originates from localized explosion centers in the failure wave, where sufficient instabilities are maintained and eventually amplify to sustain the detonation propagation front in the open area. In more recent investigations, Pintgen & Shepherd [14] described detonation diffraction and direct initiation as two equivalent phenomena related to the effect of unsteadiness in the reaction process. Using the Eckett *et al.* model [15], the critical condition is linked to the decay rate of the wave front velocity, itself a function of the effective mixture activation energy dictating the change in induction time for changes in the lead shock strength, and hence, the degree of coupling between the reaction front and the lead diverging shock. Although such model provides an estimation of the critical condition, the re-initiation mechanism as evidenced from experimental flow visualization [11, 14] is a consequence of local instabilities within the region between the lead shock and decoupled reaction zone, resulting in an explosion bubble that grows rapidly, sweeping through shocked, largely unreacted gas. These experimental results thus suggest that cellular instability and transverse waves remain important factors for successful detonation (re-) initiation.

Experiments were recently conducted by Mehrjoo *et al.* [16, 17] to discriminate between the two modes of failure conjectured by Lee [11] and clarify the importance of instability on the critical tube phenomenon. Two series of experiments were conducted: one by generating artificially small flow instabilities using small obstacles with different blockage ratios placed at the tube exit and the other by damping transverse instability using porous media. Results show that both generation and suppression of flow instability leads to a significant change in the critical condition for successful transmission of unstable detonations. No noticeable effect could be observed in stable, argon-diluted mixtures as these perturbations have not influenced significantly the curvature evolution over the diverging wave surface. These experiments demonstrate that the mechanism responsible for detonation failure in irregular undiluted mixtures is linked to the suppression of instabilities.

The present study furthers the understanding of the mechanism that underlies the critical tube diameter phenomenon, focusing on the failure mechanism and the effect of cellular instability in unstable mixtures with detailed experimental measurements. The role of transverse waves on the transmission outcome is thoroughly examined by imposing flow perturbations. Quantitative data are obtained through direct visualization using simultaneous high-speed Schlieren imaging and smoked foil technique to analyze the wave front evolution.

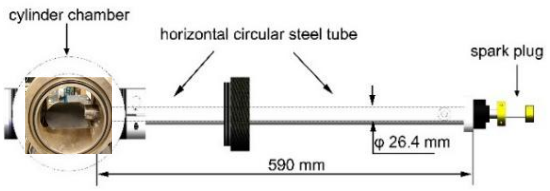

Fig. 1. Schematic of the experimental setup.

2. Experimental setup

The experimental setup, described schematically in Fig. 1, consists of a 590-mm long, circular, steel tube with an inner diameter D = 26.4 mm connected to a larger cylindrical chamber with a 125-mm inner diameter and 108-mm depth. The chamber has two opposed windows to permit Schlieren photography. A CJ detonation, initiated at the closed end of the tube via a high-voltage capacitor spark discharge, transitioned into the larger chamber. A photo probe was mounted near the end of the tube for signal triggering and ensuring from the detonation time-of-arrival a CJ detonation was fully established. High-speed Schlieren videos, with a maximum frame rate of 200 kfps and shutter speed of 10^{-6} s, were taken using a Z-type configuration setup, together with the Photron FASTCAM SA1.1 high-speed camera and the Oriel Apex 200 Watts Hg(Xe) Arc lamp as the light source. The video resolution was 128×112 pixels with an exposure time of 1 μs.

A stoichiometric C_2H_2/O_2 mixture was considered in this study. This mixture without dilution exhibits an irregular cellular detonation pattern and is often referred to in experiments as an unstable mixture [7, 18]. The mixture sensitivity was controlled by varying the initial pressure, p_o, in the range 3

– 10 kPa. The mixture was prepared in a separate vessel by the method of partial pressures and the gases were allowed to mix for at least 24 hr to ensure homogeneity of the mixture. The detonation cell size was also measured simultaneously in some tests, along with the Schlieren photography, using thin metal sheets coated with soot and inserted in the center of the tube as shown in Fig. 1. To define the critical pressure/diameter, twelve shots were repeated at each initial pressure. If a re-initiation event occurred, the initial pressure was decreased by 0.1 kPa until no re-initiation event occurred in those twelve trials.

3. Results and Discussion

3. 1. The three regimes of detonation diffraction

Schlieren photographs illustrating the three transition regimes are given in Fig. 2. For the subcritical case, a decaying diverging shock is followed by a decoupled reaction front leading to detonation failure. For the supercritical case, the detonation wave transmits seamlessly and continues to propagate into the unconfined area. For the critical case $D \sim D_c$, a decoupled reaction front is generated due to the expansion waves. Some of the original cellular transverse structure persists, creating a local explosion bubble. A new transverse detonation is formed sweeping through the pretreated gas mixture toward the wall. The experimental observation is consistent with the numerical findings reported in [19].

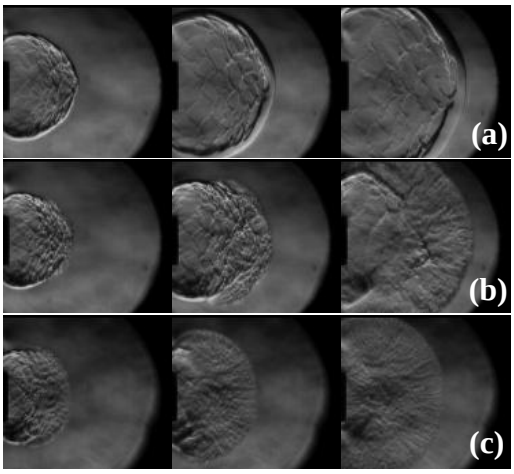

Fig. 2. The three transmission regimes: a) Subcritical (4 kPa); b) Critical (6.5 kPa); and c) supercritical (9 kPa).

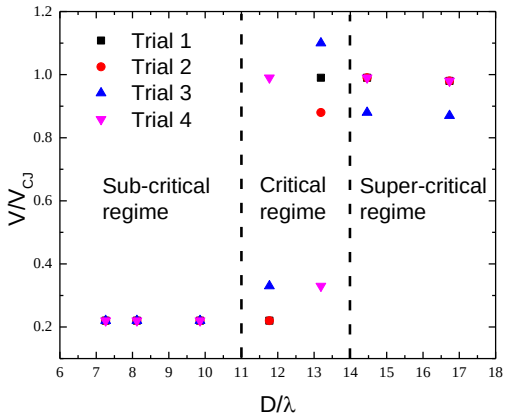

Fig. 3. Normalized velocity at different D/λ showing different transition regimes.

Sample results processed from the Schlieren still images are summarized in Fig. 3, showing the normalized axial reaction wave velocity over the CJ velocity versus the tube diameter over the detonation cell size. The cell sizes λ at each initial pressure were measured again in this study from the smoked foils. The critical regime ranges from 6 to 7 kPa, with the corresponding D/λ close to 13, in agreement with the universal scaling confirmed from previous studies for a mixture of undiluted C_2H_2/O_2 [3-5]. For subcritical cases, the detonation wave failed completely and the final velocity dropped to about 0.2 V_{CJ}. Above the critical value, the wave velocity was always around the CJ velocity.

The leading shock and reaction front velocities along the tube axis are determined using a series of Schlieren video frames, shown in Fig. 4. These velocities are determined by locating the wave position and then dividing the distance between two adjacent positions by the time interval. For the subcritical case, initially both fronts propagate close to the CJ velocity. After a certain distance, both decay rapidly to about 1000 m/s and begin to decouple from each other. The final decoupled lead shock velocity is approximately 750 m/s while that of the reaction front decays to around 500 m/s. For most critical cases (e.g., Fig 2b), the leading shock front did not decouple from the reaction wave and past a certain distance both wave velocities decrease at the same decay rate to a quasi-steady velocity of 1500 m/s. Subsequently, re-initiation occurs as shown by a re-acceleration of this complex to approximately CJ velocity. For the supercritical cases, the lead shock propagating along the tube centerline is always

coupled with the reaction front. Both front velocities remain around the C-J value throughout. From the present results, it appears that the critical velocity below which the detonation fails or decouples from the reaction front is between 1000 -1500 m/s which is roughly 0.44 - 0.65 V_{CJ}. Here, it is worth noting that this approximately ½ V_{CJ} is in agreement with previous detonation initiation studies [20] that at critical conditions, the wave decays to this sub-CJ velocity prior to the onset of the detonation. Due to the high-speed camera limitations, the position measurements' precision is 0.5 mm/pixel, giving a velocity measurement uncertainty of 250 m/s.

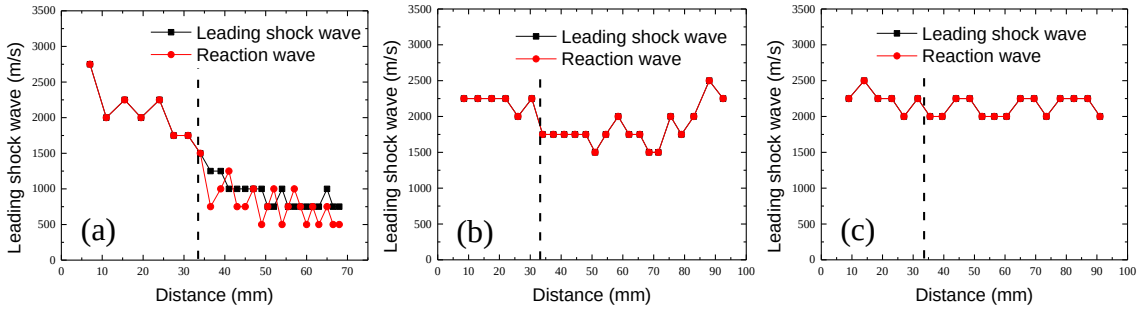

Fig. 4. Axial centerline velocity with different p_o: a) 4 kPa; b) 6.5 kPa; and c) 8 kPa. The location where the corner expansion waves reach the axis is marked by the dashed line.

Following [14, 21], Skews' geometric construction for non-reacting diffraction shocks is applied to approximate the expansion front locus created by the abrupt transition. The angle α of the corner disturbance trajectory relative to the tube axis is obtained by:

$$\tan\alpha = \frac{v}{U_s} = \frac{\sqrt{c^2 - (U_s - u)^2}}{U_s} = \frac{\sqrt{c^2 - w^2}}{U_s} \qquad (1)$$

where v is the disturbance speed propagating radially along the shock front at the local sound speed c and convected downstream at u, where u and w are the post-shock velocities in the lab and shock-fixed frames, respectively; U_s is the incoming shock velocity which is assumed to be equal to the CJ velocity U_{CJ}. The distance x_c at which the disturbance reaches the tube axis (penetration distance) is:

$$x_c = \frac{D}{2\tan\alpha} \qquad (2)$$

where D is the tube diameter. The ideal ZND model with the CHEMKIN package [22] for stoichiometric C_2H_2/O_2 is used to obtain the necessary parameters (i.e., c and u) for determining the distance x_c. Consistent with previous results [14, 21], both the perturbation angle α and the penetration distance x_c are almost independent of the initial pressure for a fixed mixture composition with only a negligible change. The distance x_c at which the head of corner disturbance, convected downstream and traveled radially outward, reaches the axis remains constant at ~33.6 mm for different initial pressures. In Fig. 4, this position is marked by a dashed line. Despite the simplicity of the model, it agrees approximately with the rapid decay of both wave fronts. For the subcritical case, the lead shock and reaction front are clearly decoupled past this position.

3. 2. Detailed characteristics of detonation failure and re-initiation

Figures 5 to 8 show the expansion cone added on the Schlieren photos and smoked foils for different initial pressures. For the subcritical case (p_o = 3 kPa) shown in Fig. 5, the head of the expansion wave is coincident with the failure wave past which detonation cells disappear from the smoked foils. The curvature induced by this corner expansion is also evident from the Schlieren images showing the decoupling between the reaction front and the diffracted shock leading to detonation failure. As p_o is increased but still within the subcritical regime, the Schlieren images indicate that with the expansion wave cone unchanged, the resulting curvature effect will not cause immediately the decoupling of the detonation wave around the tube axis. With p_o = 5 kPa shown in Fig. 6, the decay rate is slower. Even though the expansion wave has already reached the axis, the detonation is still coupled and it is only after a short distance that the detonation will be decoupled, as seen in the Schlieren photographs. Measuring from the still images, it is found that the decoupling position on the axis changes from about 30.0 to 48.0 mm when p_o varies from 3 to 6 kPa. The smoked foils show one set of triple point trajectories are not completely suppressed by the expansion wave. These only disappear a certain distance downstream from the expansion cone.

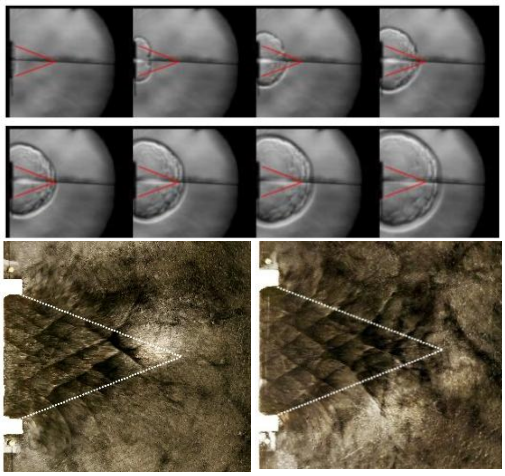

Fig. 5. Expansion cone on smoked foil and its corresponding Schlieren images with p_o = 3 kPa.

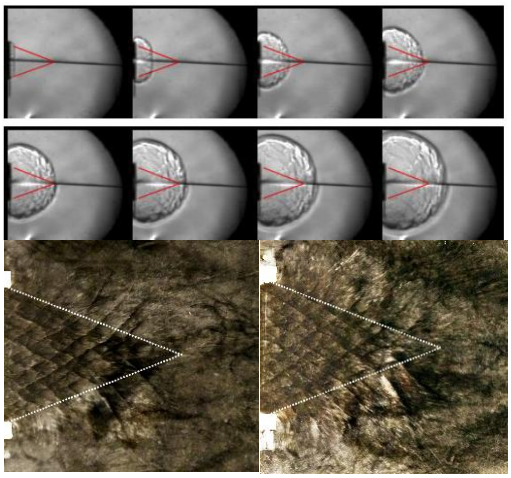

Fig. 6. Expansion cone on smoked foil and its corresponding Schlieren images with p_o = 5 kPa.

As the initial pressure approaches the critical condition of 6.5 kPa and above 7 kPa, an initial disappearance of transverse waves is first observed. A sufficient degree of cellular instabilities remains in the quasi-steady curved reaction-shock complex, i.e., outside the expansion cone. Within this flow field, a local explosion bubble is formed eventually at a location where significant flow instabilities and cellular features are still seen in the front structure (see Fig. 7 Schlieren images). The interaction of the "surviving" cellular structure with a quasi-steady shock-reaction front complex appears to be the dominant factor that controls the creation of this explosion bubble, in the curved region far from the

expansion cone. For the super-critical transition with p_o = 8 kPa (Fig. 8), although part of the diffracted detonation fails near the wall, exhibiting a disappearance of the cell structure, the failure wave trajectory does not reach the axis. The curvature induced by the expansion wave causes a slight detonation cell size growth near the tube axis, but the cellular detonation structure re-adjusts and the detonation front propagates seamlessly and engulfs the decoupled region.

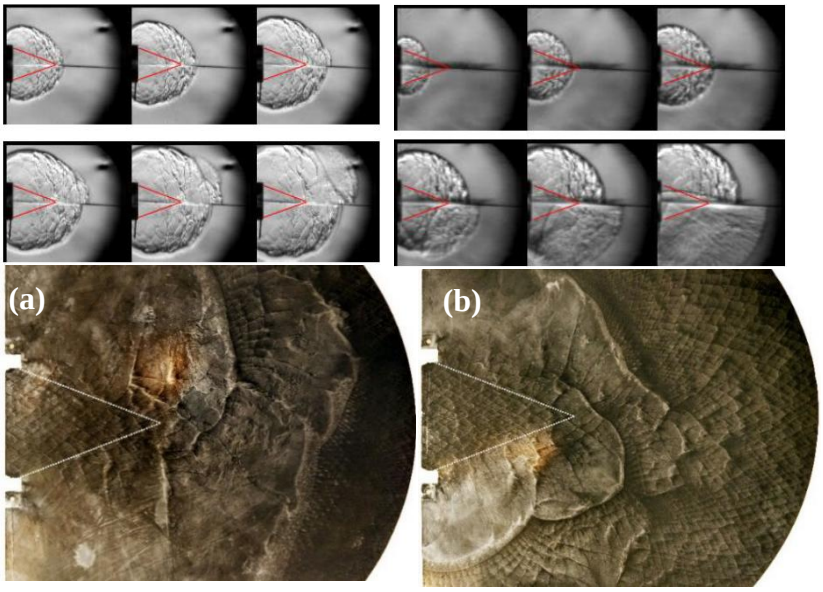

Fig. 7. Expansion cone on smoked foil and its corresponding Schlieren images with p_o = 6.5 and 7 kPa.

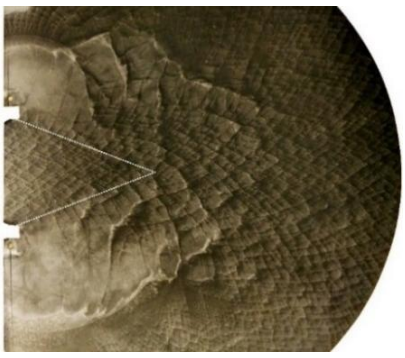

Fig. 8. Expansion cone on smoked foil with p_o = 8 kPa.

To quantify the re-initiation process, a re-initiation distance, measured from Schlieren images, is defined as the horizontal distance from the tube exit to the local explosion center. Repeated experiments

with the same conditions under a critical pressure of 6.5 kPa are used to measure this length scale. It is found that the distance is consistent at 38.9 mm ± 3 mm corresponding to 21.7λ ± 1.67λ and ~1.5*D*. Similar re-initiation length scales have been measured by Gallier *et al.* [23] and Nagura *et al.* [24]. The distance obtained from the present study is larger compared to these aforementioned two-dimensional computational and experimental results mainly due to the difference in geometry. In the present study, a circular tube was used instead of a channel.

3. 3. The effect of flow perturbations promoting instabilities

The successful transition appears to depend on the ability to maintain the cellular structure or a sufficient level of transverse wave instability. To illustrate the role of transverse wave instability on the detonation re-initiation during the detonation diffraction process, a small perturbation in the form of a thin obstacle was used to generate transverse instability in the diffracted wave. A thin sheet metal plate (8 mm × 30mm × 0.3 mm) was made as an obstacle. It is placed around the location where the local explosion bubble is observed during re-initiation at the critical regime, i.e., 39 mm. Figure 9 shows the results obtained with the perturbation. The bubble always begins from the obstacle while its position will be random if there is no obstacle. Once the diffracted lead shock reaches the obstacle, waves will be reflected and go through the weakly coupled or just decoupled shock-reaction zone region where the mixture is highly reactive. As a reflected transverse wave passes through this region, the chemical reaction is suddenly promoted. Rapid heat release causes a local explosion and produces a new transverse detonation.

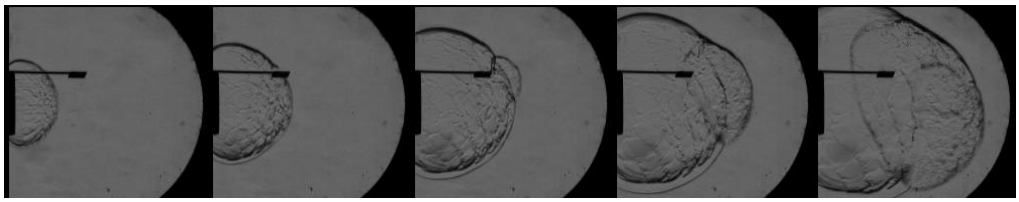

Fig. 9. Schlieren images showing the effect of perturbation with p_o = 5.1 kPa.

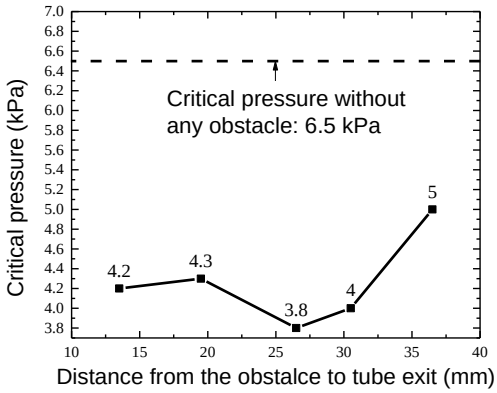

Fig. 10. The critical pressures corresponding to different distances.

The critical pressures corresponding to different perturbation distances are given in Fig. 10. With the disturbance, the critical p_o decreases from 6.5 to 5 kPa. With reducing obstacle distance, the critical pressure decreases. The lowest critical pressure is 3.8 kPa, which corresponds to a distance of 26.5 mm. However, with further distance decreases, the critical p_o increases slightly and levels at around 4.2 kPa.

From the Schlieren images, it is found that the decoupling between the lead shock and reaction zone will occur earlier close to the tube exit with the decrease in the initial pressure. If the obstacle position is kept unchanged while the initial pressure is decreased, the imposed wave disturbance would have a negligible effect on the transition. The reflected shock wave will go through the region where the detonation wave is decoupled for a long time. Such a region is not very reactive compared with the region where the detonation front just decoupled. Therefore, the reflected shock wave would not promote the reactivity of the pretreated mixture to generate a local explosion for the detonation re-initiation.

However, if the obstacle distance is decreased along with the decrease in the initial pressure, the perturbation remains synchronized with the region where the detonation wave is just decoupled, and a local explosion will be formed. This explains why decreasing the obstacle distance can lowers the critical pressure (Fig. 10). It is worth noting that the decreasing trend of the decoupling distance slows with decreasing initial pressure. Therefore, once the initial pressure is low enough, the decoupling

position will remain unchanged, so that further obstacle distance decreases are no longer helpful for the re-initiation. This explains the insignificant change in the critical pressure at around 4.2 kPa with further obstacle distance decrease (Fig. 10). In addition, if the wave reflection by the obstacle occurs too early the lead shock-reaction structure is still strongly coupled, and there is not much pretreated mixture in the region. The explosion bubble would not be strong enough to sustainably propagate downward and help the re-initiation process. Such a local explosion is relatively weak and will be damped after it propagates into the shocked but unreacted region under subcritical pressure. Therefore further obstacle distance decreases in turn increase the critical pressure slightly.

3. 4. Numerical simulation of the flow perturbation effect

The critical transition thus clearly relies on the presence of sufficient cellular activity to promote reactions in the weakly decoupled region where the lead shock and the reaction front still propagate both at a quasi-steady velocity. The role of these cellular transverse waves is to maintain the reactivity for the pretreated mixture between these two fronts to subsequently generate an explosion bubble and re-initiation. For a simple illustration, Fig. 11 shows two-dimensional numerical simulations using reactive Euler equations with a two-step induction-reaction kinetic model [25] and the numerical method with GPU computing is detailed in [26-28]. The chosen kinetic parameters give initially an irregular cellular detonation pattern in the channel. To mimic the present experiment, a small obstacle is placed near the critical region of the flow field to promote flow instabilities, see the red arrow in Fig. 11(b). When the diffracted wave emerging from the confined channel interacts with this small obstacle, reflected waves will be generated and interact with each other, increasing the degree of instability in the flow field. Without sufficient instabilities, detonation failure occurs in a homogeneous mixture as shown in Fig. 11(a). By imposing a small perturbation with an obstacle, as shown in Fig. 11(b), the induced wave instabilities result in local explosion bubbles. These preliminary results suggest that the instability and

strong wave activities generated by any flow disturbance (either using an obstacle or using randomly distributed inhomogeneities, i.e., concentrated reactive sources in the unconfined medium, proposed recently [29]) will have an effect in promoting the transition. The near-limit phenomena can be further investigated using such proposed platform by artificially generated instabilities in the flow field.

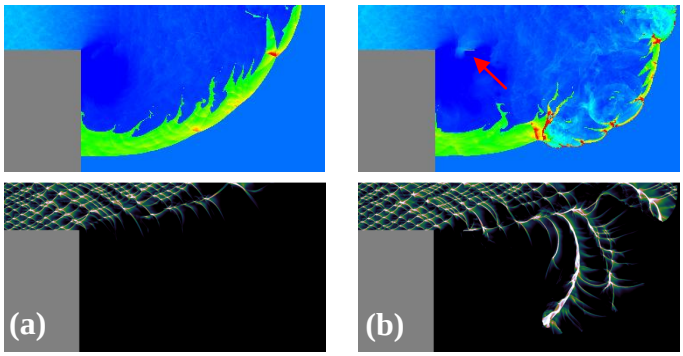

Fig. 11. Density field and numerical soot foils showing: a) the subcritical regime in a homogeneous mixture; and b) the critical transition with an obstacle perturbation indicated by the red arrow.

4. Conclusion

By simultaneously recording smoked foils and Schlieren photography, this work provides flow visualization of the three transition regimes, and elucidates the role of cellular instability on the critical tube diameter problem for unstable, gaseous detonation waves. The results show that near the critical regime, a sufficient degree of cellular instability remains in the quasi-steady, weakly decoupled curved reaction-shock complex persisting away from the expansion cone to subsequently generate an explosion bubble and re-initiation. The location of this critical zone is identified at about 22λ. To illustrate the importance of transverse instability at the diffracted front, artificial perturbations introduced by inserting a small obstacle have been shown to promote the generation of transverse waves and a re-initiation kernel. Equivalently, preliminary numerical simulations with a small obstacle placed in the unconfined reactive medium, generating additional pressure waves in the flow field upon the interaction with the

diverging wave front, also illustrate the role of cellular instability on the detonation transition into an unconfined area.

Acknowledgement

This research is supported by the China Scholarship Council (No. 201606250047) and the Natural Sciences and Engineering Research Council of Canada (NSERC).

References

1. G.D. Roy, S.M. Frolov, A.A. Borisov, D.W. Netzer, *Prog. Energy Combust. Sci.* 30 (2004) 545-672.
2. Y.B. Zeldovich, S.M. Kogarko, N.N. Simonov, Sov. Phys. Tech. Phys. 1(8) (1956) 1689-1713
3. V.V. Mitrofanov, R.I. Soloukhin, Sov. Phys.-Dokl. 9(12) (1965) 1055-1058.
4. R. Knystautas, J.H.S. Lee, C. Guirao, Combust. Flame 48 (1982) 63-83.
5. H. Matsui, J.H.S. Lee, Proc. Combust. Inst. 17 (1978) 1269-1280.
6. A.A. Vasil'ev, Combust. Expl. Shock Waves 34(4) (1998) 433-437.
7. M.I. Radulescu, The Propagation and Failure Mechanism of Gaseous Detonations: Experiments in Porous-Walled Tubes. PhD thesis, McGill University, Montreal, Canada, 2003.
8. J.E. Shepherd, I. Moen, S. Murray, P.I. Thibault, Proc. Combust. Inst. 21 (1986) 1649–1658.
9. I. Moen, A. Sulmistras, G.O. Thomas, D. Bjerketvedt, P. Thibault, Prog. Astro. Aero. 106 (1986) 220-243.
10. D. Desbordes, C. Guerraud, L. Hamada, H.N. Presles, Prog. Astro. Aero. 153 (1993) 347-359.
11. J.H.S. Lee, in: J.R. Bowen (Ed.), Dynamics of Exothermicity, Gordon and Breech Publishers, Netherlands, 1996, p. 321-336.
12. J. Li, J. Ning, C.B. Kiyanda, H.D. Ng, Prop. Power Res. 5(3) (2016) 177-183.
13. L.T. He, P. Clavin, J. Fluid Mech. 277 (1994) 227-248.
14. F. Pintgen, J.E. Shepherd, Combust. Flame 156 (3) (2009) 665-677.
15. C.A. Eckett, J.J. Quirk, J.E. Shepherd, J. Fluid Mech. 421 (2000) 147-183

16. N. Mehrjoo, B. Zhang, R. Portaro, H.D. Ng, J.H.S. Lee, Shock Waves 24 (2) (2014) 219-229.
17. N. Mehrjoo, Y. Gao, C.B. Kiyanda, H.D. Ng, J.H.S. Lee, Proc. Combust. Inst. 35 (2) (2015) 1981-1987.
18. M.I. Radulescu, H.D. Ng, J.H.S. Lee, B. Varatharajan, Proc. Combust. Inst. 29 (2) (2002) 2825-2831.
19. M. Arienti, J.E. Shepherd, J. Fluid Mech. 529 (2005) 117-146.
20. J.H.S. Lee, The Detonation Phenomenon, Cambridge University Press, Cambridge, U.K., 2008.
21. E. Schultz, Detonation Diffraction through an Abrupt Area Expansion. Ph.D. thesis, California Institute of Technology, Pasadena, USA, 2000.
22. R.J. Kee, F.M. Rupley, J. A. Miller, A Fortran Chemical Kinetics Package for the Analysis of Gas-Phase Chemical Kinetics. Report No. SAND89-8009, Sandia National Laboratories, 1989.
23. S. Gallier, F. Le Palud, F. Pintgen, R. Mevel, J.E. Shepherd, Proc. Combust. Inst. 36 (2) (2017) 2781-2789.
24. Y. Nagura, J. Kasahara, Y. Sugiyama, A. Matsuo, Proc. Combust. Inst., 34 (2013) 1949-1956
25. H.D. Ng, M.I. Radulescu, A.J. Higgins, N. Nikiforakis, J.H.S. Lee, Combust. Theory Model. 9 (3) (2005) 385-401.
26. E.F. Toro, Riemann Solvers and Numerical Methods for Fluid Dynamics, 3rd edn. Springer, Berlin, 2009.
27. C.B. Kiyanda, G.H. Morgan, N. Nikiforakis, H.D. Ng, J. Vis. 18 (2) (2015) 273-276.
28. X.C. Mi, A.J. Higgins , H.D. Ng, C.B. Kiyanda, N. Nikiforakis, Phys. Rev. Fluids 2 (2017) 053201.
29. X.C. Mi, E.V. Timofeev, A.J. Higgins, J. Fluid Mech. 817 (2017) 306-338.

Figure caption

Figure 1. Schematic of the experimental setup.

Figure 2. The three transmission regimes: a) Subcritical (4 kPa); b) Critical (6.5 kPa); and c) supercritical (9 kPa).

Figure 3. Normalized velocity at different D/λ showing different transition regimes.

Figure 4. Axial centerline velocity with different p_o: a) 4 kPa; b) 6.5 kPa; and c) 8 kPa. The location where the corner expansion waves reach the axis is marked by the dashed line.

Figure 5. Expansion cone on smoked foil and its corresponding Schlieren images with p_o = 3 kPa.

Figure 6. Expansion cone on smoked foil and its corresponding Schlieren images with p_o = 5 kPa.

Figure 7. Expansion cone on smoked foil and its corresponding Schlieren images with p_o = 6.5 and 7 kPa.

Figure 8. Expansion cone on smoked foil with p_o = 8 kPa.

Figure 9. Schlieren images showing the effect of perturbation with p_o = 5.1 kPa.

Figure 10. The critical pressures corresponding to different distances.

Figure 11. Density field and numerical soot foils showing: a) the subcritical regime in a homogeneous mixture; and b) the critical transition with an obstacle perturbation indicated by the red arrow.

Figure

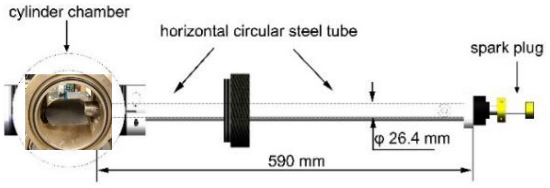
cylinder chamber
horizontal circular steel tube
spark plug
φ 26.4 mm
590 mm

Fig. 1.

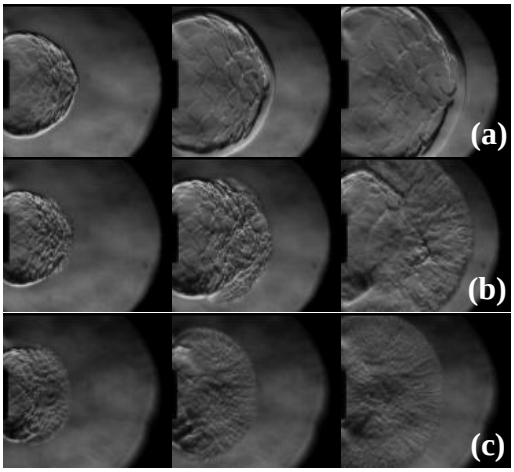

Fig. 2.

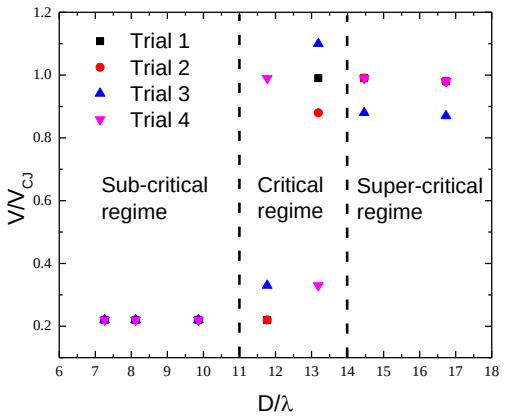
Trial 1
Trial 2
Trial 3
Trial 4
Sub-critical regime
Critical regime
Super-critical regime
V/V_CJ
D/λ
1.2
1.0
0.8
0.6
0.4
0.2
6
7
8
9
10
11
12
13
14
15
16
17
18

Fig. 3.

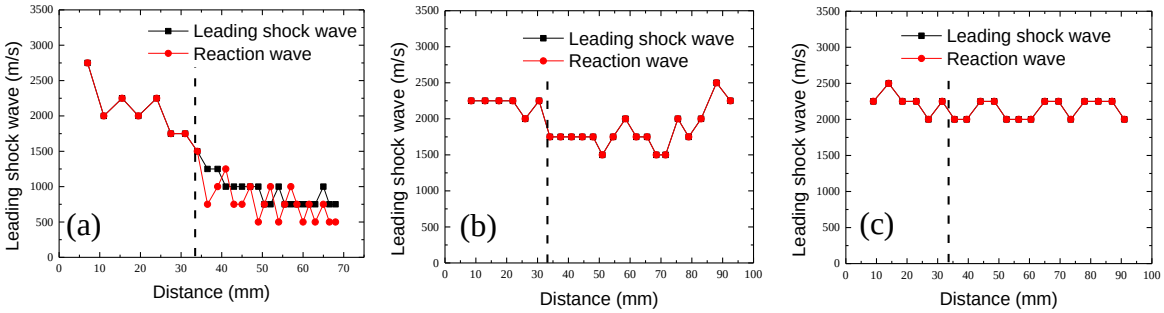
Leading shock wave
Reaction wave
Leading shock wave (m/s)
Distance (mm)
(a)
(b)
(c)

Fig. 4.

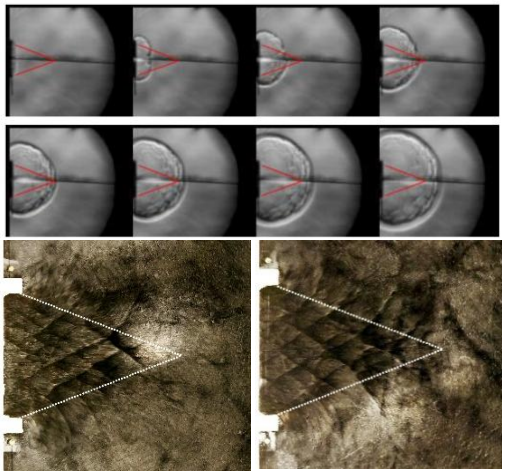

Fig. 5.

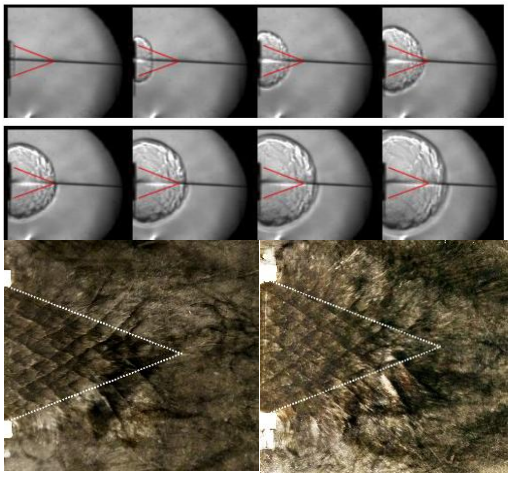

Fig. 6.

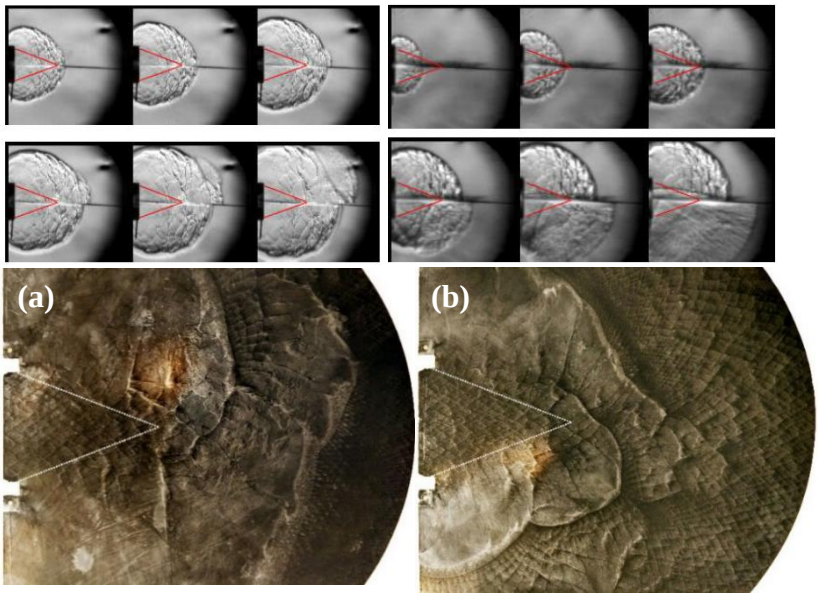

Fig. 7.

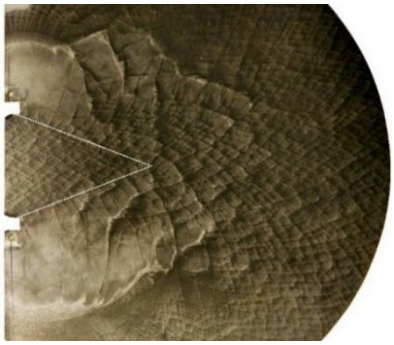

Fig. 8.

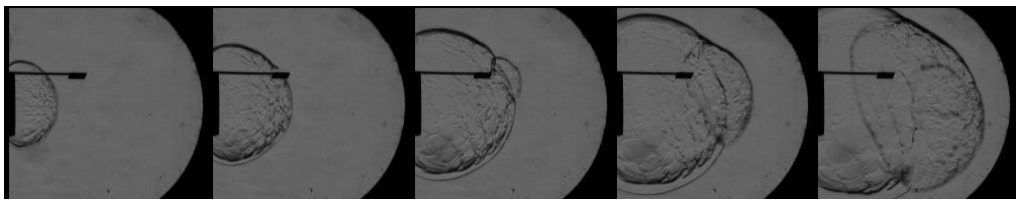

Fig. 9.

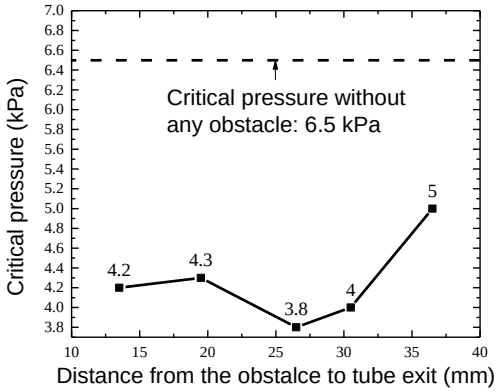
Critical pressure without
any obstacle: 6.5 kPa
Critical pressure (kPa)
Distance from the obstalce to tube exit (mm)
4.2
4.3
3.8
4
5

Fig. 10.

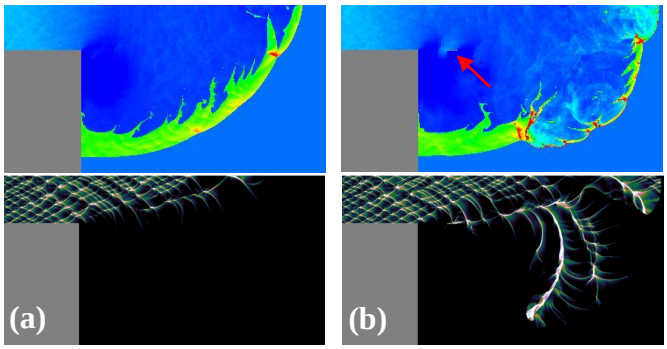

Fig. 11.